GLUENet: Ultrasound Elastography Using Convolutional Neural Network

Md. Golam Kibria[1(✉)] and Hassan Rivaz[1,2(✉)]

[1] Concordia University, Montreal, QC, Canada
m_kibri@encs.concordia.ca, hrivaz@ece.concordia.ca
[2] PERFORM Centre, Montreal, QC, Canada

Abstract. Displacement estimation is a critical step in ultrasound elastography and failing to estimate displacement correctly can result in large errors in strain images. As conventional ultrasound elastography techniques suffer from decorrelation noise, they are prone to fail in estimating displacement between echo signals obtained during tissue deformations. This study proposes a novel elastography technique which addresses the decorrelation in estimating displacement field. We call our method GLUENet (GLobal Ultrasound Elastography Network) which uses deep Convolutional Neural Network (CNN) to get a coarse but robust time-delay estimation between two ultrasound images. This displacement is later used for formulating a nonlinear cost function which incorporates similarity of RF data intensity and prior information of estimated displacement [3]. By optimizing this cost function, we calculate the finer displacement exploiting all the information of all the samples of RF data simultaneously. The coarse displacement estimate generated by CNN is substantially more robust than the Dynamic Programming (DP) technique used in GLUE for finding the coarse displacement estimates. Our results validate that GLUENet outperforms GLUE in simulation, phantom and *in-vivo* experiments.

Keywords: Convolutional neural network · Ultrasound elastography
Time-delay estimation · TDE · Deep learning · Global elastography

1 Introduction

Ultrasound elastography can provide mechanical properties of tissue in real-time, and as such, has an important role in point-of-care ultrasound. Estimation of tissue deformation is very important in elastography, and further has numerous other applications such as thermal imaging [9] and echocardiography [1].

Over the last two decades, many techniques have been reported for estimating tissue deformation using ultrasound. The most common approach is window-based methods with cross-correlation matching techniques. Some reported these techniques in temporal domain [5,10,14] while others reported in spectral domain

D. Stoyanov et al. (Eds.): POCUS 2018/BIVPCS 2018/CuRIOUS 2018/CPM 2018,
LNCS 11042, pp. 21–28, 2018.
https://doi.org/10.1007/978-3-030-01045-4_3

[8,11]. Another notable approach for estimating tissue deformation is usage of dynamic programming with regularization and analytic minimization [3,12]. All these approaches may fail when severe decorrelation noise exists between ultrasound images.

Tissue deformation estimation in ultrasound images is an analogous to the optical flow estimation problem in computer vision. The structure and elastic property of tissue impose the fact that tissue deformation must contain some degree of continuity. Hence, tissue deformation estimation can be considered as a special case of optical flow estimation which is not bound by structural continuity. Apart from many state-of-the-art conventional approaches for optical flow estimation, very recently notable success has been reported at using deep learning network for end-to-end optical flow estimation. Deep learning networks enjoy the benefit of very fast calculation by trained (fine-tuned) weights of the network while having a trade-off of long-time computationally exhaustive training phase. Deep learning has been recently applied to estimation of elasticity from displacement data [4]. A promising recent network called FlowNet 2.0 [6] has achieved up to 140 fps at optical flow estimation. These facts indicate the potential for using deep learning for tissue deformation estimation.

This work takes advantage of the fast FlowNet 2.0 architecture to estimate an initial time delay estimation which is robust from decorrelation noise. This initial estimation is then fine-tuned by optimizing a global cost function [3]. We call our method GLUENet (GLobal Ultrasound Elastography Network) and show that it has many advantages over conventional methods. The most important one would be the robustness of the method to severe decorrelation noise between ultrasound images.

2 Methods

The proposed method calculates the time delay between two radio-frequency (RF) ultrasound scans which are correlated by a displacement field in two phases combining fast and robust convolutional neural network with the more accurate global optimization based coarse to fine displacement estimation. This combination is possible due to the fact that the global optimization-based method depends on coarse but robust displacement estimation which CNN can provide readily and more robustly than any other state-of-the-art elastography method.

Optical flow estimation in computer vision and tissue displacement estimation in ultrasound elastography share common challenges. Therefore, optical flow estimation techniques can be used for tissue displacement estimation for ultrasound elastography. The latest CNN that can estimate optical flow with competitive accuracy with the state-of-the-art conventional methods is called FlowNet 2.0 [6]. This network is an improved version of its predecessor FlowNet [2], wherein Dosovitskiy et al. trained two basic networks namely FlowNetS and FlowNetC for optical flow prediction. FlowNetC is a customized network for optical flow estimation whereas FlowNetS is rather a generic network. The details of these networks can be found in [2]. These networks were further improved for more accuracy in [6] which is known as FlowNet 2.0.

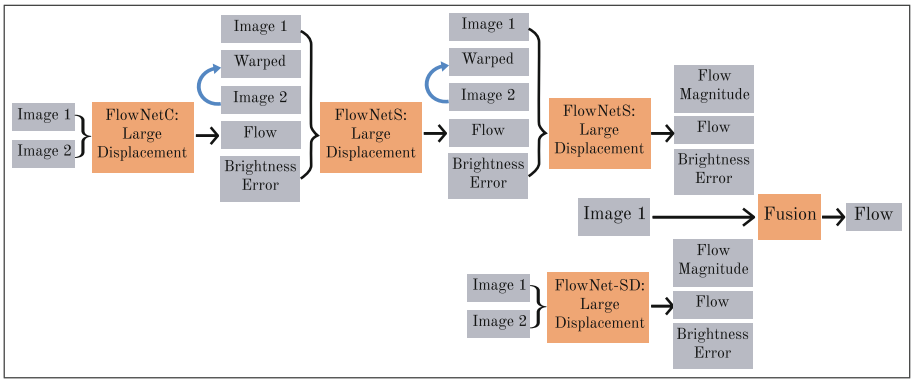

Fig. 1. Full schematic of FlowNet 2.0 architecture: The initial network input is Image 1 and Image 2. The input of the subsequent networks includes the image pairs, previously estimated flow, Image 2 warped with the flow, and residual of Image 1 and warped image (Brightness error). Input data is concatenated (indicated by braces).

Figure 1 illustrates the complete schematic of FlowNet 2.0 architecture. It can be considered as the stacked version of a combination of FlowNetC and FlowNetS architectures which help the network to calculate large displacement optical flow. For dealing with the small displacements, small strides were introduced in the beginning of the FlowNetS architecture. In addition to that, convolution layers were introduced between upconvolutions for smoothing. Finally, the final flow is estimated using a fusion network. The details can be found in [6].

The displacement estimation from FlowNet 2.0 is robust but needs more refinement in order to produce strain images of high quality. Global Time-Delay Estimation (GLUE) [3] is an accurate displacement estimation method provided that an initial coarse displacement estimation is available. If the initial displacement estimation contains large errors, then GLUE may fail to produce accurate fine displacement estimation. GLUE refines the initial displacement estimation by optimizing a cost function incorporating both amplitude similarity and displacement continuity. It is noteworthy that the cost function is formulated for the entire image unlike its motivational previous work [12] where only a single RF line is optimized. The details of the cost function and its optimization can be found in [3]. After displacement refinement, strain image is obtained by using least square or a Kalman filter [12].

3 Results

GLUENet is evaluated using simulation and experimental phantom, and *in-vivo* patient data. The simulation phantom contains a soft inclusion in the middle and the corresponding displacement is calculated using Finite Element Method (FEM) by ABAQUS Software (Providence, RI). For ultrasound simulation, the Field II software package [7] is used. A CIRS breast phantom (Norfolk, VA) is

used as the experimental phantom. RF data is acquired using an Antares Siemens system (Issaquah, WA) at the center frequency of 6.67 MHz with a VF10-5 linear array at a sampling rate of 40 MHz. For clinical study, we used *in-vivo* data of three patients. These patients were undergoing open surgical RF thermal ablation for primary or secondary liver cancer. The *in-vivo* data were collected at John Hopkins Hospital. Details of the data acquisition are available in [12]. For comparison of the robustness of our method, we use mathematical metrics such as Mean Structural Similarity Index (MSSIM) [13], Signal to Noise Ratio (SNR) and Contrast to Noise Ratio (CNR). Among them, MSSIM incorporates luminance, contrast, and structural similarity between ground truth and estimated strain images which makes it an excellent indicator of perceived image quality.

3.1 Simulation Results

Field II RF data with strains ranging from 0.5% to 7% are simulated, and uniformly distributed random noise with PSNR of 12.7 dB is added to the RF data. The additional noise is for illustrating the robustness of the method to decorrelation noise given that simulation does not model out-of-plane motion of the probe, complex biological motion, and electronic noise. Figure 2(a) shows ground truth axial strain and (b–c) shows axial strains generated by GLUE and GLUENet respectively at 2% applied strain. Figure 2(d–f) illustrates the comparable performance of GLUENet against GLUE [3] in terms of MSSIM, SNR and CNR respectively.

3.2 Experimental Phantom Results

Figure 3(a–b) shows axial strains of the CIRS phantom generated by GLUE and GLUENet respectively. The large blue and red windows in Fig. 3(a–b) are used as target and background windows for calculating SNR and CNR (Table 1). The small windows are moved to create a total combination of 120 window pairs (6 as target and 20 as background) for calculating CNR values. The histogram of these CNR values is plotted in Fig. 3(c) to provide a more comprehensive view which shows that GLUENet has a high frequency at high CNR values while GLUE is highly frequent at lower values. We test both methods on 62 pre- and post- compression RF signal pairs chosen from 20 RF signals of CIRS phantom for a measure of consistency. The best among the estimated strain images is visually marked to compare with other strain images using Normalized Cross Correlation (NCC). A threshold at 0.6 is used to determine failure rate of the methods (Table 1). GLUENet shows very low failure rate (19.3548%) compared to GLUE (58.0645%) which indicates greater consistency of GLUENet.

3.3 Clinical Results

Figure 4 shows axial strains of patient 1–3 from GLUE and GLUENet and histogram of CNR values. Similar to experimental phantom data, small target and

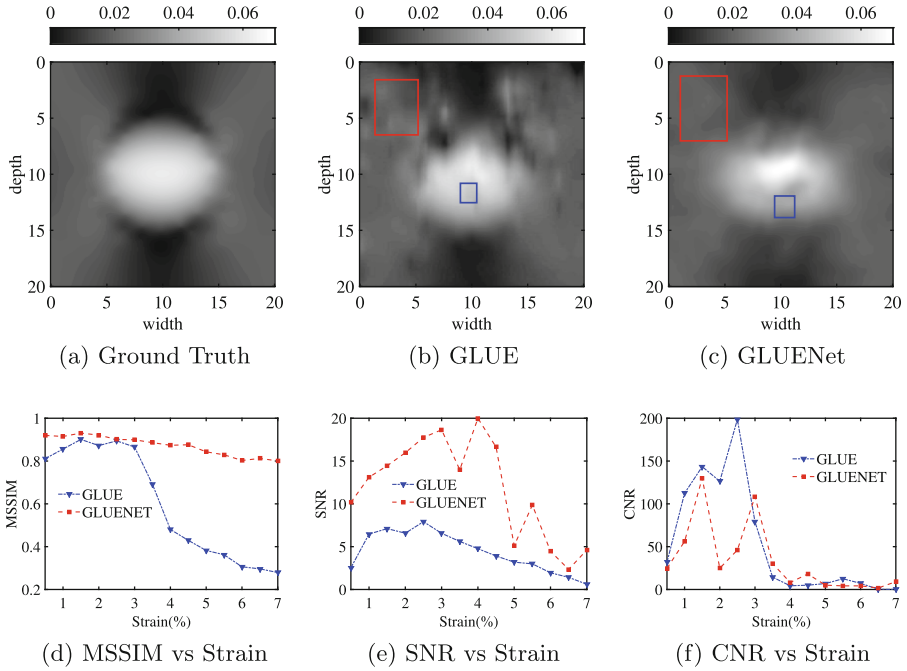

Fig. 2. First row shows axial strain images of simulation phantom with added random noise (PSNR: 12.7 dB); (a) Ground truth, (b) GLUE and (c) GLUENet. Second row shows the performance metrics graph with respect to various range of applied strain; (d) MSSIM vs Strain, (e) SNR vs Strain and (f) CNR vs Strain.

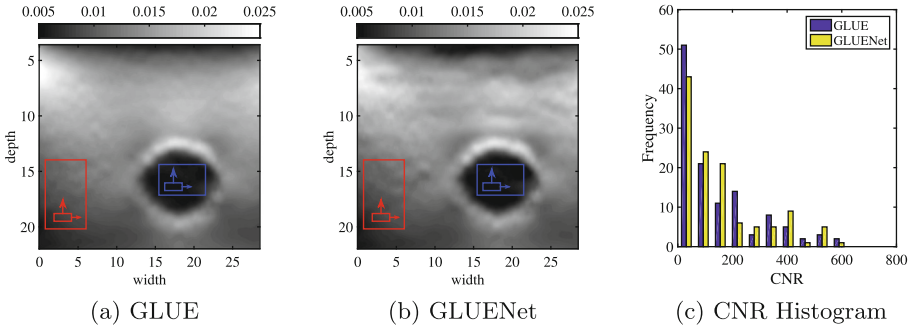

Fig. 3. Axial strain images of experimental phantom data generated by (a) GLUE and (b) GLUENet, and (c) histogram of CNR values of GLUE and GLUENet. (Color figure online)

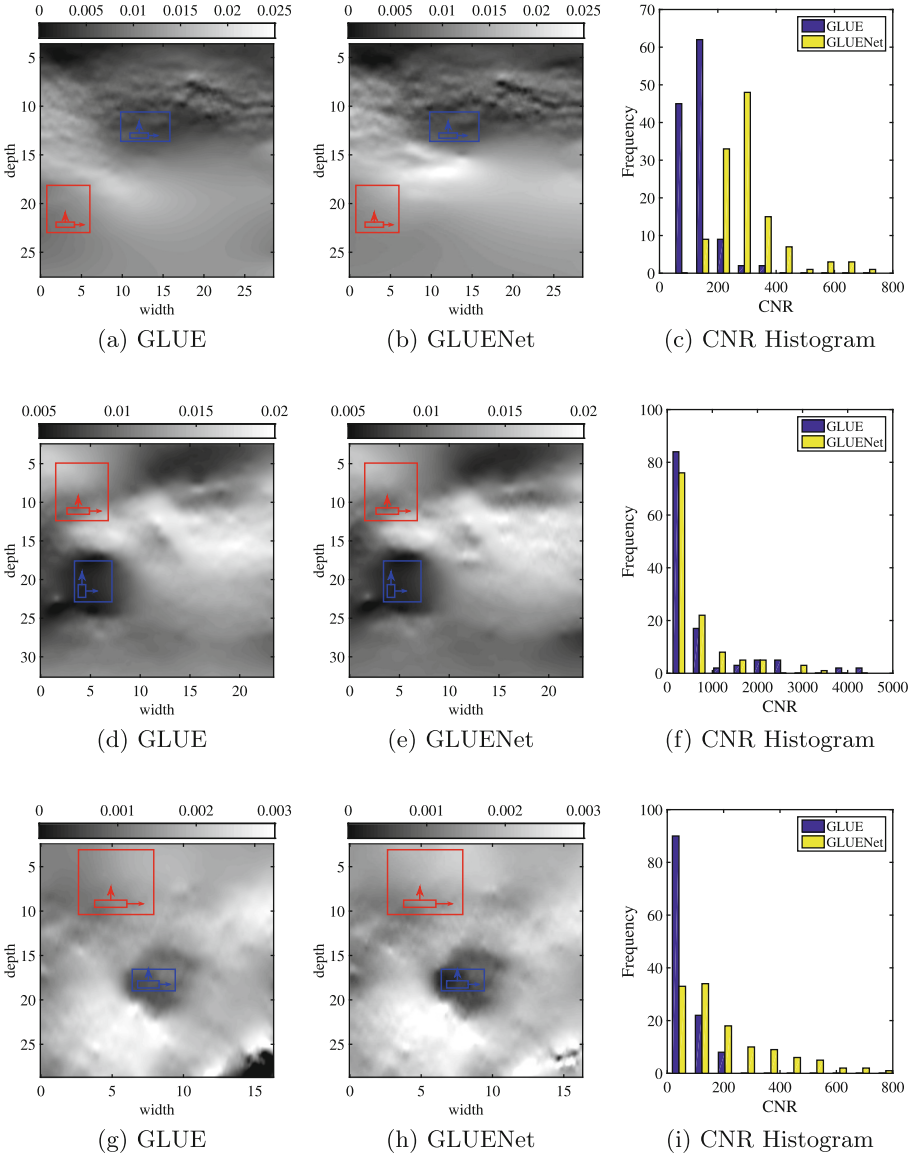

(a) GLUE (b) GLUENet (c) CNR Histogram

(d) GLUE (e) GLUENet (f) CNR Histogram

(g) GLUE (h) GLUENet (i) CNR Histogram

Fig. 4. Axial strain images of patients and histogram of CNR values: The three rows correspond to patients 1–3 respectively. First and second columns depict axial strain images from GLUE and GLUENet respectively. Third column shows histogram of CNR values of GLUE and GLUENet. (Color figure online)

Table 1. SNR and CNR of the strain images, and failure rate of GLUE and GLUENet for experimental phantom data and *in-vivo* data of patients 1–3.

	GLUE			GLUENet		
	SNR	CNR	Failure rate (%)	SNR	CNR	Failure rate (%)
Phantom	39.0363	12.6588	58.0645	43.4363	15.5291	19.3548
Patient 1	53.9914	22.1641	34.6939	54.7700	27.9264	04.8469
Patient 2	47.5051	22.7523	68.3673	55.9494	25.4911	14.5408
Patient 3	31.2440	07.7831	77.0408	28.6152	19.6954	60.7143

background windows are moved to create a total combination of 120 window pairs for calculating CNR values. Their histogram shows that GLUENet has a high frequency at high CNR values while GLUE is more frequent at low values. Table 1 shows the SNR and CNR values for all patients which is calculated by using the large blue and red windows as target and background. We calculate failure rate of GLUE and GLUENet from 392 pre- and post- compression RF echo frame pairs chosen from 60 RF echo frames of all three patients. The best axial strain is marked visually to compare with other strains using NCC. A threshold of 0.6 is used to determine the failure rate of the methods shown in Table 1. The failure rate of GLUENet is very low compared to GLUE for all patient data thus proving the robustness of GLUENet to decorrelation noise in clinical data.

The failure rates of GLUE in Table 1 are generally high because no parameter tuning is performed for the hyperparameters. Another reason for high failure rates is that we select pairs of frames that are temporally far from each other to test the robustness at extreme levels. This substantially increases non-axial motion of the probe and complex biological motions, which leads to severe decorrelation in the RF signal. In real-life, the failure rate of these methods can be improved by selecting pairs of RF data that are not temporally far from each other.

4 Conclusions

In this paper, we introduced a novel technique to calculate tissue displacement from ultrasound images using CNN. This is, to the best of our knowledge, the first use of CNN for estimation of displacement in ultrasound elastography. The displacement estimation obtained from CNN was further refined using GLUE [3], and therefore, we referred to our method as GLUENet. We showed that GLUENet is robust to decorrelation noise in simulation, experiments and *in-vivo* data, which makes it a good candidate for clinical use. In addition, the high robustness to noise allows elastography to be performed by less experienced sonographers as a point-of-care imaging tool.

Acknowledgement. This research has been supported in part by NSERC Discovery Grant (RGPIN-2015-04136). We would like to thank Microsoft Azure Research for a cloud computing grant and NVIDIA for GPU donation. The ultrasound data was collected at Johns Hopkins Hospital. The principal investigators were Drs. E. Boctor, M. Choti, and G. Hager. We thank them for sharing the data with us.

References

1. Amundsen, B.H., et al.: Noninvasive myocardial strain measurement by speckle tracking echocardiography: validation against sonomicrometry and tagged magnetic resonance imaging. J. Am. Coll. Cardiol. **47**(4), 789–793 (2006)
2. Dosovitskiy, A., et al.: FlowNet: learning optical flow with convolutional networks. In: Proceedings of the IEEE International Conference on Computer Vision, pp. 2758–2766 (2015)
3. Hashemi, H.S., Rivaz, H.: Global time-delay estimation in ultrasound elastography. IEEE Trans. Ultrason. Ferroelectr. Freq. Control **64**(10), 1625–1636 (2017)
4. Hoerig, C., Ghaboussi, J., Insana, M.F.: An information-based machine learning approach to elasticity imaging. Biomech. Model Mechanobiol. **16**(3), 805–822 (2017)
5. Hussain, M.A., Anas, E.M.A., Alam, S.K., Lee, S.Y., Hasan, M.K.: Direct and gradient-based average strain estimation by using weighted nearest neighbor cross-correlation peaks. IEEE TUFFC **59**(8), 1713–1728 (2012)
6. Ilg, E., Mayer, N., Saikia, T., Keuper, M., Dosovitskiy, A., Brox, T.: FlowNet 2.0: evolution of optical flow estimation with deep networks. In: IEEE Conference on Computer Vision and Pattern Recognition (CVPR), vol. 2 (2017)
7. Jensen, J.A.: FIELD: a program for simulating ultrasound systems. Med. Biol. Eng. Comput. **34**(suppl. 1, pt. 1), 351–353 (1996)
8. Kibria, M.G., Hasan, M.K.: A class of kernel based real-time elastography algorithms. Ultrasonics **61**, 88–102 (2015)
9. Kim, Y., Audigier, C., Ziegle, J., Friebe, M., Boctor, E.M.: Ultrasound thermal monitoring with an external ultrasound source for customized bipolar RF ablation shapes. IJCARS **13**(6), 815–826 (2018)
10. Ophir, J., et al.: Elastography: imaging the elastic properties of soft tissues with ultrasound. J. Med. Ultra. **29**(4), 155–171 (2002)
11. Pesavento, A., Perrey, C., Krueger, M., Ermert, H.: A time-efficient and accurate strain estimation concept for ultrasonic elastography using iterative phase zero estimation. IEEE TUFFC **46**(5), 1057–1067 (1999)
12. Rivaz, H., Boctor, E.M., Choti, M.A., Hager, G.D.: Real-time regularized ultrasound elastography. IEEE Trans. Med. Imaging **30**(4), 928–945 (2011)
13. Wang, Z., Bovik, A.C., Sheikh, H.R., Simoncelli, E.P.: Image quality assessment: from error visibility to structural similarity. IEEE TIP **13**(4), 600–612 (2004)
14. Zahiri-Azar, R., Salcudean, S.E.: Motion estimation in ultrasound images using time domain cross correlation. IEEE TMB **53**(10), 1990–2000 (2006)